Chin. J. Geochem. (2015) 34(3):346–361
DOI 10.1007/s11631-015-0057-3

ORIGINAL ARTICLE

Discussion on the PGE anomalies and source materials of K-bentonite (Bed 5) in the Lower Cambrian Meishucun section, Yunnan

Lecai Xing[1,2] · Mingzhong Zhou[3] · Liang Qi[1] · Zhilong Huang[1]

Received: 16 February 2015 / Revised: 13 March 2015 / Accepted: 20 May 2015 / Published online: 7 June 2015

Abstract The Meishucun section in Yunnan is the stratotype section for stratigraphic correlation of the Lower Cambrian strata across the Yangtze Block. Known for enriched small shelly fossils, it is a prominent section for investigating the Early Cambrian phosphogenic event. Pašava et al. (Econ Geol 105:1047–1056, 2010) reported anomalously high PGE concentrations in this section, up to 576×10^{-9} (434×10^{-9} Pt, 142×10^{-9} Pd) for the total PGE concentrations of a K-bentonite sampled from the bottom of Bed 5. This finding can illustrate two significant statements: (1) in addition to the attested polymetallic Ni-Mo-PGE ore layer, another potential PGE enrichment layer exists with PGE concentrations up to the mineralization level; and (2) acid volcanics have high PGE contents overturning conventional views. To inspect whether the anomalous PGE concentration is pervasive, we investigated Bed 5 of the Meishucun section systematically, and sampled from a profile with a thickness of 3.5 m. The major and trace element geochemistry indicate the Bed 5 K-bentonite is derived from acid volcanic ash. PGE concentrations were determined repeatedly by isotope dilution-ICP-MS using improved digestion technique (Qi et al., in J Anal At Spectrom 26:1900–1904, 2011), and were duplicated by fire assay method. The results showed that each sample had total PGE concentrations of less than 0.90×10^{-9}, and Pt + Pd concentrations of no higher than 0.70×10^{-9}. Combined with the petrological and mineralogical features, and trace and rare earth element analyses, it is inferred that no generality of PGE enrichment exists in Bed 5 and that the anomalous PGE concentration is likely due to the nugget effect of volcanic ash modified by currents in a shallow coastal environment.

Keywords Platinum group elements (PGEs) · K-Bentonite · The Meishucun section · The Lower Cambrian

1 Introduction

The Meishucun section in Yunnan is located in the district of the Kunyang Phosphorite Mine, Southwest Kunming, which is the stratotype section for correlation of the Lower Cambrian strata in southwestern China (Luo et al. 1984; Qian et al. 1984). It was proposed as the candidate stratotype section for the Precambrian/Cambrian boundary (Cowie 1985; Luo et al. 1985, 1994). Therefore, it has received extensive attention from scholars worldwide. This section contains well-developed Precambrian-Cambrian sedimentary successions and consists of shallow marine dolostones, phosphorites, shales, and siltstones, characterized by various fossils (e.g. small shelly fossils, trace fossils, acritarchs, and microfossils) (Song 1984; Cowie 1985; Luo et al. 1985; Brasier et al. 1990) and massive phosphorites. It is one of the most important sections for studies of paleontology, stratigraphy, and phosphogenic events. Luo et al. (1985) suggested the Lower Cambrian strata of this section are enriched in well-preserved small shelly fossils and associated trace fossils which facilitated

✉ Mingzhong Zhou
mingzhongzhou@126.com

[1] State Key Laboratory of Ore Deposit Geochemistry, Institute of Geochemistry, Chinese Academy of Sciences, Guiyang 550002, China

[2] University of Chinese Academy of Sciences, Beijing 100049, China

[3] School of Geographical and Environmental Sciences, Guizhou Normal University, Guiyang 550001, China

regional stratigraphic correlation and attracted numerous research projects on the subdivision of small shelly fossils in the Meishucun section (Crimes and Jiang 1986; Brasier et al. 1990; Steiner et al. 2007; Parkhaev and Demidenko 2010). The phosphorite body of the Meishucun section occurs in the Zhongyicun Member of the Lower Cambrian Zhujiaqing Formation with an average thickness about 11.6 m and is one of the largest phosphorite deposits in the Lower Cambrian strata in China (Xu et al. 2014). Thus, the Meishucun section becomes an important section for studying the Early Cambrian phosphogenic event. According to previous research, the phosphorites were deposited in a shallow marine environment (Zeng and Yang 1987; Yang et al. 1995, 2011), the formation of which was primarily induced by paleotectonics and biological activities (Zeng et al. 1989; Shen et al. 2000). Meanwhile, this worldwide phosphogenic event may have exerted considerable influence on biological evolution, promoting an increase in total shallow marine biomass, faunal diversification, precipitation of skeletons, and explosive evolution (Cook and Shergold 1984).

Bed 5 of the Meishucun section mainly consists of K-bentonites, which are favorable dating materials and an important record of Early Cambrian volcanic activity. This K-bentonite was initially dated at 525 ± 7 Ma (Compston et al. 1992), and later modified at 538.2 ± 3 Ma (Jenkins et al. 2002), 539.4 ± 2.9 Ma (Compston et al. 2008), and 536.5 ± 2.5 Ma (Sawaki et al. 2008). Based on four Nano-SIMS measurements (Sawaki et al. 2008) and 13 concordant SIMS measurements, a grand mean $^{206}Pb/^{238}U$ age of 535.2 ± 1.7 Ma was calculated and considered the best estimate for this K-bentonite (Zhu et al. 2009). Due to the lack of igneous rocks and scarce fossil records in outcrops of the deep-water facies of the Lower Cambrian in South China, the discovery and detailed research of volcanic activity records preserved in strata have important scientific significance: (1) to determine the relative age order of volcanic activity and tectonic setting, facilitating regional correlation of strata; and (2) to provide new clues for material sources of the Lower Cambrian polymetallic Ni-Mo-PGE layer in South China (Zhou et al. 2011, 2014). Detailed geochemical work on several K-bentonite beds in multiple Lower Cambrian sections (including Bed 5 of the Meishucun section) has indicated that Early Cambrian volcanic activity in South China is related to intraplate extension (Zhang et al. 1997; Zhou et al. 2011, 2014). In related research, the two Lower Cambrian K-bentonite layers (Bed 5 and the bottom of Bed 9) across the Yangtze platform have been correlated (Zhou et al. 2014). Zhou et al. (2011) suggested that the K-bentonite layers (equivalent to Bed 9 bottom bentonite of the Meishucun section) discovered in the Lower Cambrian section in Zunyi, Guizhou Province can provide new clues for the material sources of the Lower Cambrian polymetallic Ni-Mo-PGE layer in South China. Typically, Bed 5 of the Meishucun section and its equivalent layers lie up to several meters to tens meters below the polymetallic Ni-Mo-PGE layer (Chen et al. 2009; Zhu et al. 2009; Zhou et al. 2013). Detailed geochemical research of this layer, especially PGE studies, have important significance in determining the material sources of the polymetallic Ni-Mo-PGE layer.

Pašava et al. (2010) analyzed the PGE of Bed 5 K-bentonite of the Meishucun section. The sample KU-1 was from the bottom of this K-bentonite layer (Fig. 2). PGE concentrations were pre-concentrated using fire-assay fusion and measured by inductively coupled plasma mass spectrometry (ICP-MS) at the Faculty of Science, Charles University, Prague. Pt and Pd concentrations were duplicated in the ACME labs, Canada. The original rock of KU-1 was acid tuff, with anomalously high PGE concentrations: $\sum$PGEs $\geq 576 \times 10^{-9}$, Pt 434×10^{-9}, and Pd 142×10^{-9} (Table 4). Anomalous PGE enrichment is generally associated with basic-ultrabasic magma activity, and has no relevance to acid magma activity. Moreover, there is no other report of great PGE enrichment in acid rocks besides Pašava et al. (2010). Assuming the results of the Meishucun section have a commonality, namely this layer enriches PGEs, this discovery not only serves as an example of PGE-enriched acid rocks, providing important reference for the sources of PGEs in the polymetallic Ni-Mo-PGE layer above this layer; but also implies that Bed 5 of the Meishucun section will become a new type for PGE mineralization. If so, this discovery will have important significance for mineral resources and ore deposit research. For this reason, the generality of PGEs anomalies in Pašava et al. (2010) should be confirmed. In the present work, more detailed PGE geochemical analyses were carried out for Bed 5 of the Meishucun section. Results revealed that the PGE concentrations of all samples are rather lower ($\sum$PGEs $<0.90 \times 10^{-9}$, Pt + Pd $\leq 0.70 \times 10^{-9}$). It can be concluded that the anomalous enrichment of PGEs found by Pašava et al. (2010) is not a generality.

2 Geological setting

The Meishucun section of Jinning town is located in the district of the Kunyang Phosphorite Mine about 45 km southwest Kunming, Yunnan, and is geologically on the south flank of the Xiangtiaochong anticline, on the southwest margin of the Yangtze platform, and is part of the Ediacaran (Sinian)—Lower Cambrian sedimentary successions (Fig. 1). Its paleogeographic location during the late Sinian–Early Cambrian period was a second-order platform near the margin of the Oldland (Luo et al. 1984). Based on field observations and previous work on the

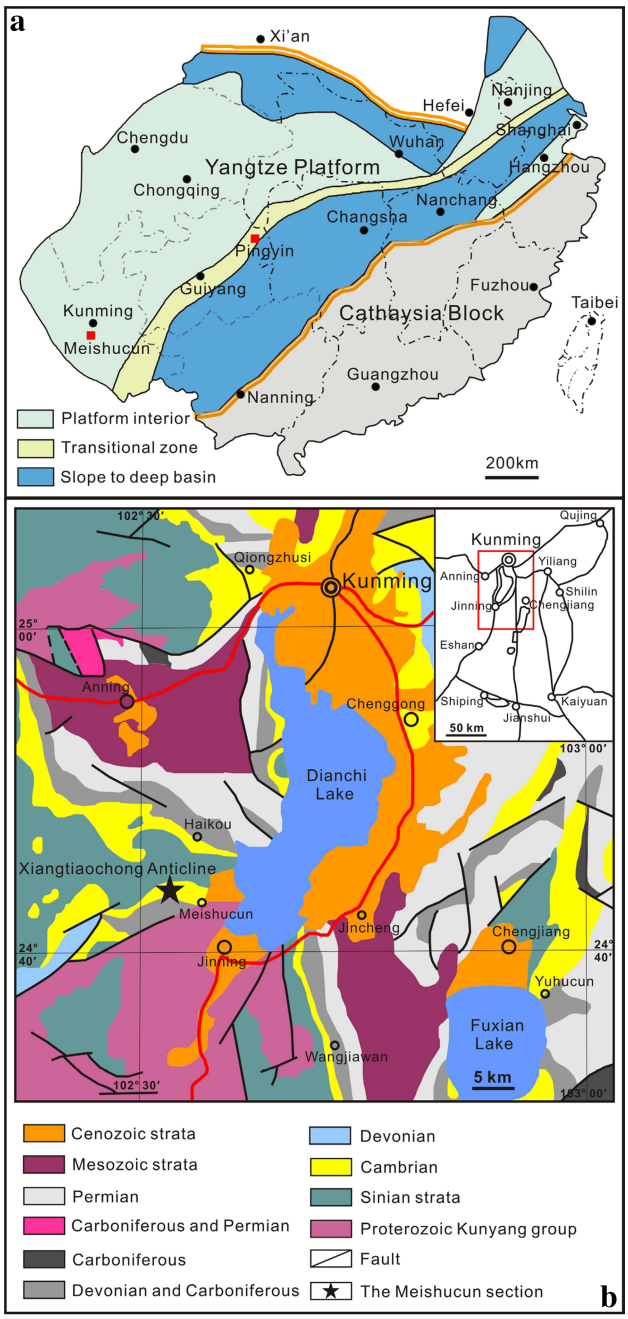

Fig. 1 Simplified palaeogeographic map of the Yangtze Platform during the Early Cambrian (**a** modified after Jiang et al. 2007; Zhou et al. 2013 and geological map of the Kunming region in Yunnan Province, showing the location of the Meishucun section in the Kunyang Phosphorite Mine, **b** modified after Pašava et al. 2010)

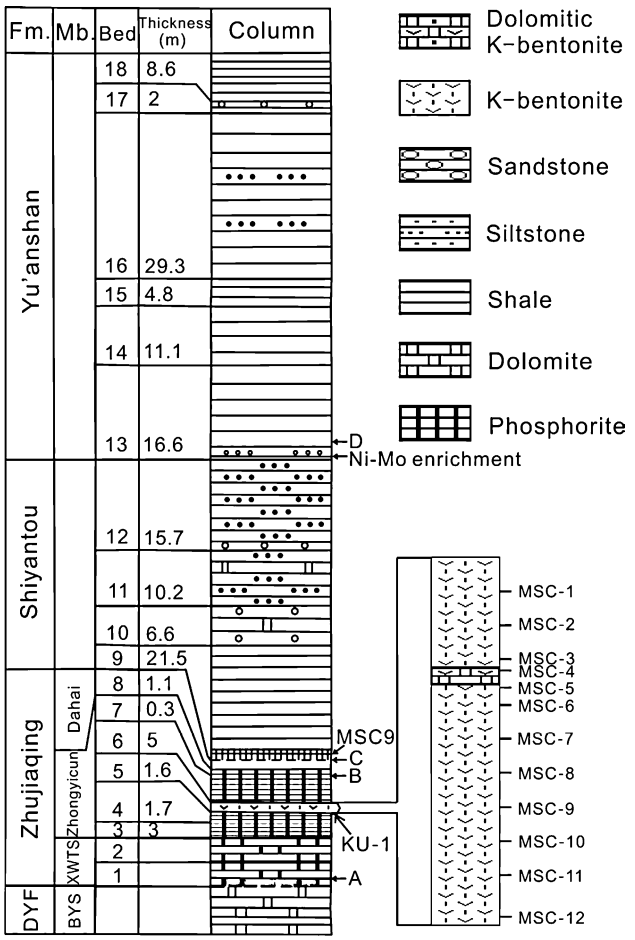

Fig. 2 Stratigraphic column of the Lower Cambrian sequences in Kunming region showing the sample locations in the Meishucun section (modified after Pašava et al. 2010). As shown in figure, Bed 5 is a K-bentonite layer between Bed 6 and Bed 7, which divides the phosphorite into *upper* and *lower* parts; between Bed 8 and Bed 10, Bed 9 is dominantly comprised of *black shale* and has phosphate laminae overlain by a thin K-bentonite layer at its *bottom*

stratigraphy of the Meishucun section, the lithostratigraphic column is shown in Fig. 2. The Lower Cambrian strata of the Meishucun section is divided into three formations, containing 18 beds: the Zhujiaqing (Beds 1–8), Shiyantou (Beds 9–12), and Yuanshan Formations (Beds 13–18). The Zhujiaqing Formation is subdivided into three members: the Xiaowaitoushan, Zhongyicun, and Dahai Members, in ascending order. Unconformably overlying the Sinian Dengying Formation, the Xiaowaitoushan Member of the Cambrian Zhujiaqing Formation consists of gray massive sandy dolostones, containing chert bands and small shelly fossils occurring 0.8 m above the bottom (Qian et al. 1984; Luo et al. 1985, 1991). It is generally considered that Marker A (see in Fig. 2) is the Precambrian-Cambrian boundary (Zhu et al. 2009). The Zhongyicun Member consists mainly of phosphorite and is enriched in various fossils. A claystone layer (Bed 5) is interbedded in the middle part of this member, by which the phosphorite is divided into the upper and the lower parts. The upper phosphorite deposit can be subdivided into two layers, namely Bed 6 and 7, with Marker B of small shelly fossils abruptly blooming at the boundary of the two beds (Luo et al. 1991). The Dahai Member is dominantly comprised of grey sandy dolostone, also containing small shelly fossils

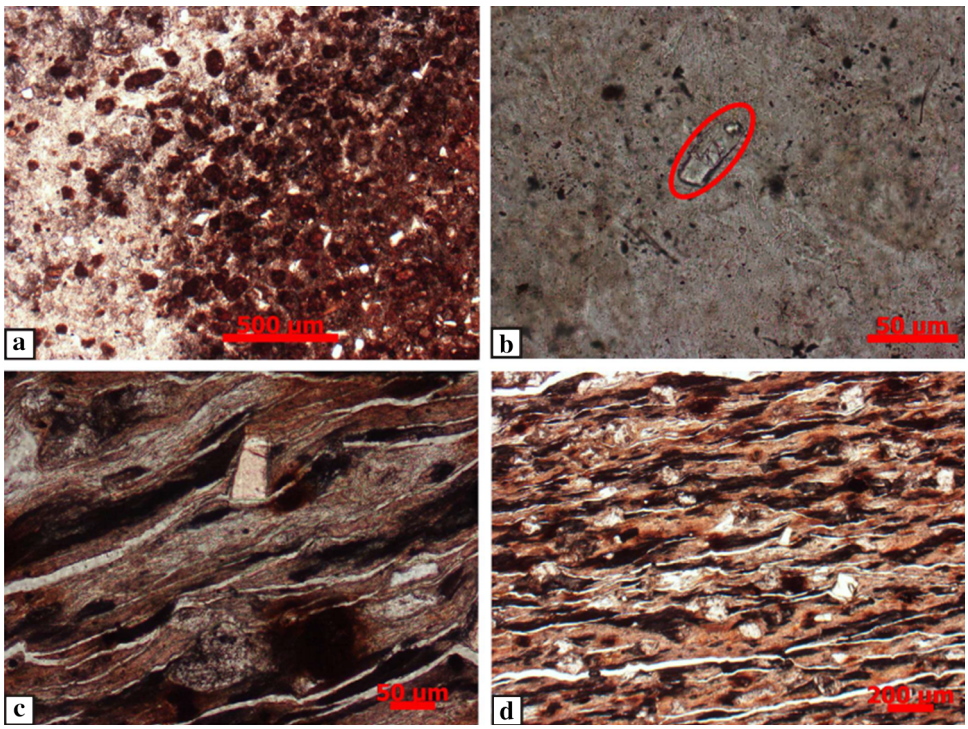

Fig. 3 Microscopic characteristics of the K-bentonites from Bed 5 and the *bottom* of Bed 9 in the Meishucun section in Kunyang Phosphorite Mine, Yunnan. **a**, **b** The clasts of phosphates and crystal fragments (sanidine phenocryst), respectively, in samples from the K-bentonite layer (Bed 5); **c**, **d** The pseudofluidal structure and crystal fragments in samples from the K-bentonite layer (the *bottom* of Bed 9)

(Luo et al. 1985). The Shiyantou Formation mainly consists of the lower black shale, and the middle and upper grey siltstone, unconformably overlying the Dahai Member, and the boundary of the two is usually recorded as Marker C (Zhu et al. 2009). The Yuanshan Formation mainly consists of shale, siltstone, and silty shale. The polymetallic Ni-Mo-PGE layer is in the basal black shale of this formation (Zhu et al. 2003; Zhou et al. 2008). The oldest trilobite occurs at Marker D, 2.4 m above the bottom boundary (Luo et al. 1991), and the well-known Chengjiang fauna are preserved in the middle siltstone.

Bed 5 of the Meishucun section wholly occurs as off-white to dark grey, massive, locally containing pyrite nodules and developing off-white dolomitic laminae or lenses, containing fossils. The average thickness of this bed is 1.6 m. This bed was previously described as "white mud layer" (Qian et al. 1984), P-containing claystone, or argillaceous shale (Qian et al. 1984; Luo et al. 1985). Bed 9 of this section is comprised of *black shale*, commonly known as "lower black layer," with an average thickness of 21.5 m. A yellowish claystone layer no more than 10 cm thick with obvious weathering characteristics occurs at the bottom of this bed. Previous researches suggest that the two claystone layers of Bed 5 and the bottom of Bed 9 in the Meishucun section are derived from tuffaceous materials deposited in marine environments, which were subsequently hydrolyzed and altered, forming smectite-enriched bentonite and mixed-layered illite–smectite and illite-enriched metabentonite or K-bentonite (Zhang et al. 1997; Zhou et al. 2007). Due to the typical enrichment of K in these metabentonites—$K_2O > 3.5$ %—many researchers refer to these rocks as K-bentonites (Su et al. 2003; Luo et al. 2005; Zhou et al. 2007), and so do we in this paper.

3 Sampling and analysis methods

3.1 Sampling and petrological characters

The thickness of the K-bentonite (Bed 5) of the middle of the Zhongyicun member, Zhujiaqing Formation in the Meishucun section varies dramatically (0.5–4.5 m across the Kunyang Phosphorite Mine), with an average thickness of 1.6 m. Samples were taken from the fresh profile of the open pit of the Kunyang Phosphorite Mine. The thickness of Bed 5 at the sampling profile in this study is about 3.5 m. A total of 12 samples were sampled from Bed 5 of this profile from top to bottom, at 30 cm intervals (Fig. 2). In comparison, MSC9 was sampled from the apparently weathered yellowish K-bentonite (about 10 cm thick) at the bottom of Bed 9 of the Shiyantou Formation. The surfaces of MSC-1 and MSC-5 from Bed 5 were slightly weathered and yellowish. MSC-4 had partly undergone barite mineralization. All others were fresh samples. Bed 5 samples (except MSC-4) mainly consist of clay minerals, with minor phosphate debris (Fig. 3a), crystal fragments (Fig. 3b), and pyrites. These clay minerals are dominantly comprised of illites, mixed-layered illite–smectites, and

kaolinites (Zhang et al. 1997). Non-clay minerals are biotites and quartz fragments (Zhu et al. 2009), with zircons occasionally. MSC9 has pseudorhyolitic structure and is mainly comprised of clay minerals, with minor crystal fragments and zircons occasionally (Zhou et al. 2014); the clay mineral composition of MSC9 is identical to that of Bed 5 (Zhang et al. 1997).

3.2 Analytical methods

Samples were first crushed into small fragments, and then ground into powders (<200 mesh) for major element, trace element, and PGE analyses. Major element analysis was carried out at ALS Laboratory Group, Guangzhou, China, using Lithium borate fusion method, and the contents were determined by Axios X-ray fluorescence spectrometry (XRF), with an analytical precision of better than 5 %. Trace element analysis was carried out at State Key Laboratory of Ore Deposit Geochemistry, Institute of Geochemistry, Chinese Academy of Sciences, by EIAN6000 ICP-MS with standard reference materials of OU-6 and GB-PG-1 for data quality monitoring, and analytical precision better than 5 %. The detailed analytical procedure is given by Qi et al. (2000). PGEs were also analyzed in State Key Laboratory of Ore Deposit Geochemistry, Institute of Geochemistry, Chinese Academy of Sciences, using improved digestion method for the determination of PGEs in rock samples Qi et al. (2011): five grams of powdered sample were put into 120 ml PTEE sealed beaker, dissolved at 185 °C by HF and HNO_3. PGEs were pre-concentrated by Te coprecipitation method. Interfering elements including Cu, Ni, Zr, and Hf are separated by cation exchange resin and P507 levextrel resin (Qi et al. 2004, 2007). Finally, PGE concentrations were determined by ELAN6000 ICP-MS. Blank and reference material analyses were carried out by the same experimental procedure.

Due to the low PGE concentrations in samples, the certainty of data were ensured by: (1) twelve samples of Bed 5 were analyzed at least twice (thrice for a few samples) by the same method and procedure (see details in Qi et al. 2011). (2) PGE analyses (primarily for Pt and Pd) of an aliquot of these powdered samples were duplicated at ALS Laboratory Group (ALS Mineral-ALS Chemex), Guangzhou, China, by fire-assay fusion method (30 g sample powder) and ICP-MS. (3) To best eliminate the nugget effect and ensure data quality, all 12 powdered samples of Bed 5 were disproportionately mixed, ground again, and mixed sufficiently. Then the mixed sample (MSC5-M) of Bed 5 K-bentonite of the Meishucun section was repeatedly analyzed (see detailed procedure in Qi et al. 2011).

4 Results

4.1 Major and trace elements

Major element concentrations are listed in Table 1. In this study, SiO_2 content of Bed 5 samples of the Meishucun section is in the range of 61.60–74.20 %, with an average of 65.89 %, belonging to intermediate-acid igneous rocks. The SiO_2 content of MSC-4 (74.20 %) is highest, similar to KU-1 (71.57 %). Contents of Al_2O_3 are in the range of 7.87–15.40 %, with an average of 13.10 %, wherein the Al_2O_3 of MSC-4 (7.87 %) has an apparent minimum value. The K_2O contents of the samples vary only slightly, in the range of 4.84–5.68 %, with an average of 5.40 % and are consistent with the previous knowledge that K_2O contents of K-bentonites are generally larger than 3.5 % (Zhou et al. 2007). P_2O_5 content ranges from 0.78 to 1.3 %, with an average of 0.98 %. The contents of Fe_2O_3, Na_2O, TiO_2, are 0.74–1.63, 0.03–0.05, and 0.07–0.13 %, respectively. MnO contents are 0.01 %, with that of MSC-1 <0.01 %. Contents of most major elements (Al_2O_3, Fe_2O_3, MgO, K_2O, P_2O_5, TiO_2, MnO) of Bed 5 samples in this study are consistent with the contents reported by Zhang et al. (1997). K_2O/Na_2O ratios, from 96.80 to 180.33, are high for all samples, while TiO_2/Al_2O_3 ratios are low, from 0.007 to 0.009. TiO_2/Al_2O_3 ratios almost keep constant in diagenesis and can be used to effectively indicate material sources, for example, ratios of TiO_2/Al_2O_3 of acid volcanic rocks are below 0.02, while TiO_2/Al_2O_3 of shales are in the range of 0.035–0.05 (Zhang et al. 1997). TiO_2/Al_2O_3 ratios of Bed 5 samples of the Meishucun section in this study are well below 0.02, apparently in the range of acid volcanic rocks.

Concentrations of trace elements and REE of samples and related references are tabulated in Table 2. A Cl-chondrite-normalized spider diagram of trace elements and REE distribution patterns are shown in Figs. 4 and 5, respectively.

Zhang et al. (1997) suggested that some trace elements are immobile in the altered and supergene environments, with slight variations, for example: Hf, Nb, Ta, Th, Y, and Ga. These elements can effectively differentiate volcanogenic claystone from non-volcanogenic claystone. In general, volcanogenic claystone has higher abundance of the elements mentioned above and of marker elements of volcanic activity (As, Se, and Sb). Compared to shale of the Earth's crust representing average crustal claystone background values (Turekian and Wedepohl 1961), Bed 5 samples of the Meishucun section have lower concentrations of trace elements (Sc, V, Cr, Co, Ni, Cu, Zn, Rb, and Sr); higher concentrations of lithophile elements (Hf, Ta, Th, and Y) and marker elements of volcanic activity; and As in the range of 17.95–33.56 $\times 10^{-6}$, about 1.3–2.6

Table 1 Major element compositions of samples from the K-bentonite layer (Bed 5) in the Meishucun section at the Kunyang Phosphorite Mine in Yunnan Province (wt%)

Sample	SiO_2	Al_2O_3	Fe_2O_3	MgO	CaO	Na_2O	K_2O	TiO_2	P_2O_5	MnO	LOI	Total	K_2O/Na_2O	TiO_2/Al_2O_3
MSC-1	68.5	14.25	1.12	2.42	1.98	0.05	5.38	0.11	1.3	<0.01	3.59	99.2	107.6	0.008
MSC-2	68.7	12.7	0.99	2.74	2.87	0.05	5.36	0.1	1.11	0.01	4.7	100.55	107.2	0.008
MSC-3	64.2	13.6	0.92	3.56	3.55	0.05	5.68	0.1	1.24	0.01	5.8	99.54	113.6	0.007
MSC-4	74.2	7.87	0.74	1.65	2.79	0.05	4.84	0.07	0.86	0.01	3.71	98.74	96.8	0.009
MSC-5	69.4	12.1	0.78	2.95	2.71	0.04	5.23	0.11	0.78	0.01	4.98	99.2	130.75	0.009
MSC-6	65	13	1.02	3.91	3.57	0.04	5.18	0.12	0.84	0.01	6.64	100.3	129.5	0.009
MSC-7	65.9	13.45	0.77	3.63	3.05	0.04	5.4	0.13	0.83	0.01	5.85	99.64	135	0.010
MSC-8	62	13.45	1.63	4.1	3.87	0.04	5.36	0.12	0.98	0.01	7.05	100.95	134	0.009
MSC-9	61.6	14.55	1.02	4.39	3.8	0.04	5.4	0.13	0.97	0.01	7	99.7	135	0.009
MSC-10	64.5	13.5	0.88	3.77	3.34	0.04	5.6	0.12	0.82	0.01	6.29	99.66	140	0.009
MSC-11	65	13.35	1.12	3.61	3.06	0.04	5.67	0.11	0.89	0.01	5.75	99.82	141.75	0.008
MSC-12	61.7	15.4	1.02	4.39	3.15	0.03	5.68	0.13	1.08	0.01	6.11	99.66	189.33	0.008
MSC5	65.89	13.10	1.00	3.43	3.15	0.04	5.40	0.11	0.98	0.01	5.62	99.75	127.02	0.009
KU-1	71.57	10.89	0.48	2.49	2.76	0.04	4.92	0.09	0.79	0.01		97.303	123	0.008
PY-13	52.39	27.86	0.54	3.32	0.19	0.24	6.99	0.11	0.15	0	8.43	100.99	29.13	0.004
K25	59.17	15.12	1.12	3.96	4.19	0.08	5.36	0.21	1.18	0.01			68.72	0.014
K27	56.17	17.41	1.07	4.77	4.01	0.078	5.23	0.14	1.8	0.01			67.05	0.008
K31	44.26	18.13	1.19	4.63	10.78	0.13	6.32	0.34	2.08	0.01			48.62	0.019
K108	53.50	23.50	3.24	3.77	0.75	0.07	6.56	0.33	0.07				93.71	0.014
K843	52.60	22.41	3.39	4.19	0.53		5.88	0.20	0.28	0.02				0.009

MSC5 represents the mean value of 12 samples from the K-bentonite layer (Bed 5) of the Meishucun section in this study; some major element data cited from references are listed in the table for comparison: KU-1 is the K-bentonite (Bed 5) sample in the Meishucun section reported by Pašava et al. (2010); PY-13 is the K-bentonite from the deeper water facies of the Pingyin section, in Jiangkou County, Guizhou Province, equivalent to Bed 5 of the Meishucun section (Zhou et al. 2013); K25, K27, and K31 are samples from Bed 5 of the Meishucun section reported by Zhang et al. (1997); K108 and K843 are K-bentonites from the bottom of Bed 9 of the Meishucun section reported by Zhang et al. (1997)

times that of shale (Table 2). Samples mostly have low Ba concentrations (169–548 $\times 10^{-6}$). However, MSC-1, MSC-4, and MSC-11 have high Ba concentrations, well above that of shale—2520 $\times 10^{-6}$, 13,600 $\times 10^{-6}$, and 1400 $\times 10^{-6}$, respectively. The high Ba concentration of MSC-4 is consistent with its petrological character of post-diagenetical barite mineralization. Rb and Sr concentrations of samples other than MSC-4 slightly vary from 65.90 $\times 10^{-6}$ to 84.30 $\times 10^{-6}$ and from 35.6 $\times 10^{-6}$ to 56.1 $\times 10^{-6}$, respectively. In contrast to other samples, MSC-4 is characterized by lower Rb (38.60 $\times 10^{-6}$) and higher Sr (94.40 $\times 10^{-6}$) concentration. In comparison to shale of the Earth's crust, the K-bentonite sample of Bed 9 bottom of the Meishucun section (MSC-9) has lower concentrations of Sc, V, Cr, Co, Ni, Cu, Zn, Rb, and Sr; higher concentrations of lithophile elements Hf, Ta, Th, U, Y; and about two times As concentrations (31.60 $\times 10^{-6}$) as shale of the Earth's crust, similar to Bed 5, and indicating acid volcanogenesis. K-bentonite of Bed 9 has an apparent weathered appearance (yellowish) and high concentrations of Rb (94.00 $\times 10^{-6}$) and Sr (7.34 $\times 10^{-6}$), notably different from Bed 5 samples.

Based on the immobility of Zr, Ti, Th, and Hf in the supergene and altered environments, Zr/Hf and Ti/Th ratios can be used to inquire into the sources of claystone. In the Meishucun section, Zr/Hf ratios of Bed 5 and Bed 9 samples are 25.48–27.51 and 19.88 respectively, both lower than shale of the Earth's crust (57.1), and similar to previously reported volcanic-sedimentary claystones (27–36.5) and tuff (37.8) (Feng and Dong 1993). Ti/Th ratios of Bed 5 are 20.03–31.31, and of the Bed 9 sample, 63.62, both considerably lower than shale of the Earth's crust (383), and again similar to acid volcanogenic claystones (30–400) (Feng 1989). According to the similar results reported in the Meishucun age K-bentonite, East Yunnan Zhang et al. (1997), it can be concluded that the primary source of K-bentonite of the studied area is acid volcanic ash.

In the Cl-chondrite-normalized spider diagram (Fig. 4), Bed 5 samples of the Meishucun section in the Kunyang Phosphorite Mine are relatively depleted in Rb, Nb, Pb, and

Table 2 Trace element and rare earth element compositions of samples from the K-bentonite layer (Bed 5) in the Meishucun section at Kunyang Phosphorite Mine in Yunnan Province ($\times 10^{-6}$)

Sample	MSC-1	MSC-2	MSC-3	MSC-4	MSC-5	MSC-6	MSC-7	MSC-8	MSC-9	MSC-10	MSC-11	MSC-12	MSC5	KU-1	PY-13	K25	K27	K31	MSC9	K108	K843	ECS
Sc	8.14	5.76	6.5	4.26	5.67	6.28	7.2	4.84	5.29	5.17	4.49	5.32	5.74		6.39				3.5			13
V	5.75	3.77	4.38	2.81	4.98	5.3	5.59	3.97	3.85	4.09	3.65	4.55	4.39		79				26.1			130
Cr	7.55	3.67	2.76	2.91	4.56	2.82	2.73	3.79	3.55	3.31	3.31	4.36	3.78		15				17.25			90
Co	3.86	4.57	4.68	17.2	8.84	4.4	3.66	2.89	3.71	3.33	3.63	2.49	5.27	0.9	3.62	3.6	2.6	2.6	1.04	3.8	5.9	19
Ni	4.48	7.17	5.77	4.17	4.19	5.89	12.7	6.92	6.4	6.2	11.6	13.2	7.39	19	36.1	9	12	8.7	7.63	14	21	68
Cu	7.22	5.86	4.93	7.32	5.68	7.53	8.18	4.57	5.65	4.77	7.96	9.79	6.62	3.8	64.8				8.97	8.8	17	45
Zn	51.3	47	46.3	43.3	49.7	42.9	15	16.6	145	10.8	12.4	12	41.03	45	93.5	53	36	70	21.3	87	151	95
Ga	22.6	18	21	7.98	18.4	20.8	21.9	19.6	20.6	18.8	18.3	21	19.08		37.8	24.4	26.2	31	40.1	44.6	46.5	19
Ge	0.82	0.77	0.85	0.74	0.72	0.76	0.78	0.71	0.67	0.6	0.61	0.63	0.72		1				0.56			1.6
As	25.75	32.43	19.51	22.29	18.47	18.9	21.51	22.89	33.56	19.86	17.95	18.3	22.62	5.4	8.61	10.8	2.4		31.6	35	26	13
Rb	72.7	65.9	78	38.6	68.7	74.9	78.4	76	78.8	72.4	72.7	84.3	71.78		173	91	99	110	94	117	109	140
Sr	56.1	46.7	48.8	94.4	38.9	39.6	39.1	41.8	40.4	35.6	37.8	39.1	46.53		22.6	55	54	42	7.34	24	13	300
Y	57.4	47.5	52.3	37.7	41	45.3	45.6	49.8	50.3	45.7	50.2	55.5	48.19		27.4	59	61	42	46.4	55	58	26
Zr	155	140	154	78.6	140	158	158	159	169	156	148	170	148.8	144.4	178	189	198	291	328	377	364	160
Nb	10.3	9.48	10.7	5.92	9.57	10.5	11.3	11.1	12.3	10.9	10	11.9	10.33		11.9	12.9	13	12	115	140	140	11
Mo	1.6	4.61	0.53	0.49	0.6	0.42	1.9	0.84	2	1.38	0.74	0.4	1.29	3.2	5.4				21.3			2.6
Ag	0.26	0.18	0.22	0.14	0.19	0.22	0.21	0.27	0.28	0.21	0.19	0.23	0.22	<0.1	0.48				2.84			0.07
Sb	1.95	2.22	1.04	1.02	1.49	0.93	1.03	1.1	1.95	0.87	0.89	1.09	1.3	0.4	0.92				4.23			1.5
Cs	15.7	12.8	17.9	4.38	14.2	18	19.1	18.3	19.7	17.1	16.8	20.9	16.24		23.7				14.9			5
Ba	2520	176	170	13,600	192	221	548	169	242	363	1400	377	1665		5920	162	162	161	215	2273	183	580
La	28	19.2	21.8	19.6	16.9	18.3	23.6	35.7	22.2	19	25.5	31.3	23.43	13.1	14.6	32	39.3	21.8	0.97	0.4	2	92
Ce	49.4	34.8	39	35.6	30.5	33.7	42.5	63.5	44.2	37.2	44.8	55.2	42.53	71.8	31.8	70.3	89.4	66.4	2.28	1.14	8.28	59
Pr	6.64	4.71	5.03	4.83	4.09	4.37	5.35	7.41	5.8	4.87	5.97	7.26	5.53	3.17	4.57	9.3	11.1	9.31	0.31	0.26	1	5.6
Nd	24.4	17.5	18.5	17.6	14.7	15.7	18.9	24.4	21.5	18.6	22.9	28.1	20.23	13.3	17.2	34.6	40.79	34.6	1.47	0.83	3.6	24
Sm	5.44	4.07	4.2	3.99	3.43	3.42	4	4.64	4.96	4.24	5.11	6.3	4.48	2.6	3.46	8.25	9	8.9	0.73	0.79	1.47	6.4
Eu	0.28	0.25	0.26	0.28	0.2	0.2	0.2	0.23	0.24	0.21	0.25	0.31	0.24	0.16	0.4	0.39	0.41	0.5	0.11	0.09	0.16	1
Gd	5.84	4.67	4.62	5.26	3.7	4.02	4.1	4.77	5	4.4	5.27	6.21	4.82	2.86	3.84	8.38	9.22	8.7	1.29	1.35	2.12	6.4
Tb	1.11	0.9	0.93	0.82	0.77	0.82	0.86	0.96	1.02	0.89	0.96	1.16	0.93	0.55	0.67	1.61	1.74	1.74	0.52	0.58	0.71	1
Dy	7.38	6.13	6.87	5.43	5.62	6.2	6.37	6.77	7.12	6.48	6.34	7.35	6.51	3.5	4.49	9.67	11	10.74	5.48	5.45	5.87	4.6
Ho	1.87	1.55	1.88	1.3	1.53	1.68	1.76	1.81	1.83	1.65	1.55	1.81	1.69	0.79	1.01				1.71			1.2
Er	5.63	4.84	5.87	3.73	4.91	5.4	5.72	5.8	5.6	5.14	4.89	5.73	5.27	2.88	2.99	7.22	7.74	6.45	6.3	6.45	6.45	2.5
Tm	0.9	0.81	0.93	0.55	0.79	0.88	0.91	0.91	0.88	0.85	0.84	0.9	0.85	0.53	0.51				1.16			0.2
Yb	6.41	5.53	6.51	3.65	5.35	5.92	6.18	6.2	5.95	5.82	5.94	6.62	5.84	3.9	3.35	8	8.19	7.74	8.92	10.6	9.29	2.6
Lu	0.96	0.82	0.97	0.55	0.8	0.9	0.93	0.89	0.85	0.86	0.91	0.98	0.87	0.61	0.49	1.18	1.16	1.0	1.29	1.6	1.35	0.7
Hf	5.75	5.38	5.82	2.98	5.24	5.9	6.2	5.98	6.16	5.67	5.52	6.27	5.57		8.24	8.6	18.6	12	16.5	19	18	2.8
Ta	1.36	1.22	1.33	0.67	1.19	1.28	1.4	1.36	1.36	1.27	1.24	1.38	1.25		3.89				11.2			0.8
Pb	11.77	72.74	7.42	57.03	70.72	18.22	10.82	15.6	17.02	12.38	6.83	5.1	25.47	4.2	20.7	9.9	8.4	12	14.1	26	67	20
Th	23.2	24.5	27.2	13.4	22.3	24.9	26.1	30.3	30.1	29.2	24.5	28.1	25.32		31.4	34	37	46	35.8	38	38	12
U	5.84	7.14	7.02	4.05	4.79	5.47	6.91	7.13	7.25	6.53	3.43	2.08	5.64	7	5	2.5	3.5	9.9	21.9	17.7	13.7	3.7

Table 2 continued

Sample	MSC-1	MSC-2	MSC-3	MSC-4	MSC-5	MSC-6	MSC-7	MSC-8	MSC-9	MSC-10	MSC-11	MSC-12	MSC5	KU-1	PY-13	K25	K27	K31	MSC9	K108	K843	ECS
Ti	659.28	599.35	599.35	419.54	659.28	719.22	779.15	719.22	779.15	719.22	659.28	779.15	674.27	539.41	659.28	1258.63	839.09	2037.79	2277.53	1977.85	1198.7	4600
∑REE	144.26	105.77	117.36	103.19	93.28	101.51	121.37	163.99	127.15	110.22	131.22	159.22	123.21	119.75	89.38	190.9	229.05	177.88	32.54	29.54	42.3	207.5
LREE	114.16	80.53	88.79	81.9	69.82	75.69	94.55	135.88	98.9	84.12	104.53	128.47	96.45	104.13	72.03	154.84	190	141.51	5.86	3.51	16.51	188.3
HREE	30.1	25.24	28.58	21.29	23.46	25.81	26.82	28.11	28.25	26.1	26.69	30.75	26.77	15.62	17.35	36.06	39.05	36.37	26.67	26.03	25.79	19.2
$\frac{\text{LREE}}{\text{HREE}}$	3.79	3.19	3.11	3.85	2.98	2.93	3.53	4.83	3.5	3.22	3.92	4.18	3.6	6.67	4.15	4.29	4.87	3.89	0.22	0.13	0.64	9.81
$(La/Yb)_N$	2.97	2.36	2.27	3.65	2.15	2.1	2.59	3.91	2.53	2.22	2.92	3.21	2.72	2.28	2.96	2.72	3.26	1.91	0.07	0.03	0.15	24.04
Ce/Ce*	0.83	0.85	0.85	0.85	0.85	0.87	0.86	0.88	0.92	0.91	0.83	0.83	0.86	2.52	0.97	1	1.04	1.25	0.98	1.07	1.64	0.35
Pr/Pr*	1.09	1.09	1.07	1.1	1.1	1.08	1.08	1.07	1.07	1.06	1.06	1.05	1.1	0.59	1.11	1.08	1.05	1.11	0.95	1.52	1.04	0.89
Eu/Eu*	0.15	0.17	0.18	0.19	0.17	0.17	0.15	0.15	0.15	0.15	0.15	0.15	0.2	0.18	0.33	0.14	0.14	0.17	0.36	0.27	0.28	0.48
Zr/Hf	26.96	26.02	26.46	26.38	26.72	26.78	25.48	26.59	27.44	27.51	26.81	27.11	26.7		21.6	21.98	10.65	24.25	19.88	19.84	20.22	57.1
Ti/Th	28.42	24.46	22.03	31.31	29.56	28.88	29.85	23.74	25.89	24.63	26.91	27.73	26.63		21	37.02	22.68	44.3	63.62	52.05	31.54	383.33
Rb/Sr	1.3	1.41	1.6	0.41	1.77	1.89	2.01	1.82	1.95	2.03	1.92	2.16	1.54		7.65	1.65	1.83	2.62	12.81	4.88	8.38	0.47

$Ce/Ce^* = 3*Ce_N/(2*La_N + Nd_N)$, $Pr/Pr^* = Pr_N/(Ce_N*Nd_N)^{0.5}$, $Eu/Eu^* = Eu_N/(Sm_N*Gd_N)^{0.5}$ (Shields and Stille 2001); $_N$ represents normalized value against the Cl chondrite (McDonough and Sun 1995); some trace element and REE data cited from references are listed in the table for comparison: KU-1 was after Pašava et al. (2010); PY-13 was after Zhou et al. (2014); K25, K27 and K31 are samples from Bed 5 of the Meishucun section reported by Zhang et al. (1997); K108 and K843 are K-bentonites from the bottom of Bed 9 of the Meishucun section reported by Zhang et al. (1997); ECS represents the continental crust shale (Turekian and Wedepohl 1961)

Sr, and enriched in Th, U, Ta, and Hf. A single sample is relatively enriched in Ba. These trace element signatures are similar to those of typical K-bentonites of different eras (Zhou et al. 2007) and wholly match the report of Zhang et al. (1997). Undergoing barite mineralization, MSC-4 has low Rb concentration, high Sr concentration, and a Rb/Sr ratio lower than other Bed 5 samples. Being subjected to weathering, K-bentonite of Bed 9 bottom has slightly high Rb concentration, considerably low Sr concentration, and a Rb/Sr ratio higher than Bed 5 samples.

The total REE concentrations of Bed 5 samples of the Meishucun section vary slightly, in the range of 93.28–163.99 $\times 10^{-6}$, with an average of 123.21 $\times 10^{-6}$. LREE/HREE and $(La/Yb)_N$ ratios both are in narrow ranges of 2.93–4.83 (average of 3.60) and 2.10–3.91 (average of 2.72), respectively. Bed 5 samples show granite-like right-tilt REE patterns indicating that LREEs are enriched while HREEs are depleted, in agreement with previous work on the same layer (Zhang et al. 1997) and equivalent layers in deeper water facies (Zhou et al. 2013) (Fig. 5). There is a slightly negative Ce anomaly and an intensively positive Eu anomaly, with Ce/Ce* ratios of 0.83–0.92 and low Eu/Eu* ratios of 0.15–0.19 (Fig. 5). Compared to Bed 5, REE of the weathered K-bentonite of Bed 9 bottom (MSC9) is characterized by heavily depleted ∑REE (32.54 $\times 10^{-6}$) and low LREE/HREE (0.22), $(La/Yb)_N$ (0.07), Ce/Ce* (0.98), and Eu/Eu* (0.36)—a conspicuously different left-tilt REE pattern in which LREE are depleted while HREE are enriched, with no Ce anomaly and the same intensively negative Eu anomaly (Fig. 5). The intensively negative Eu anomalies of all samples may either be the result of diagenesis or a signal primarily inherited from parent magmas. Previous work favors the latter (Zhou et al. 2011).

4.2 PGE

Results of the total procedural reagent blanks, reference materials and MSC5-M analyses are tabulated in Table 3. PGE concentrations of samples using the improved digestion technique and fire-assay fusion method, as well as other related samples, are shown in Table 4. Primitive-mantle-normalized PGE patterns are depicted in Fig. 8.

4.2.1 The method choice of PGE determination and data reliability

Due to the large sampling volume and effectiveness needed to overcome the nugget effect, the conventional fire-assay fusion method has been extensively applied in analysis of PGEs in geological samples. However, the total procedural reagent blank of this method is inevitably elevated by the use of reagents that, with the exception of nickel powder,

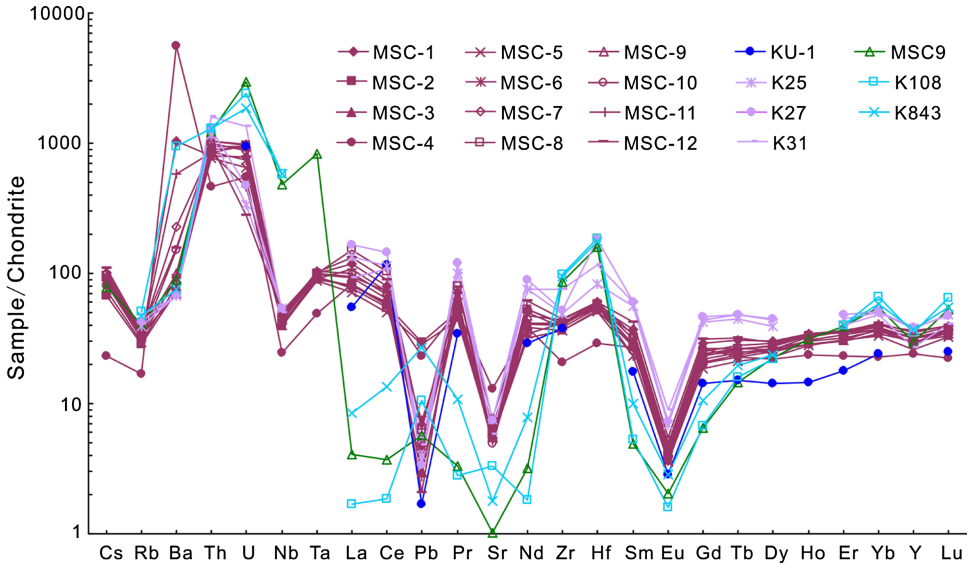

Fig. 4 Cl chondrite-normalized multi-element spider diagram of this study and the data cited for comparison (normalization values after McDonough and Sun 1995). KU-1 was after Pašava et al. (2010); K25, K27 and K31 are samples from Bed 5 of the Meishucun section reported by Zhang et al. (1997); K108 and K843 are K-bentonites from the *bottom* of Bed 9 of the Meishucun section reported by Zhang et al. (1997)

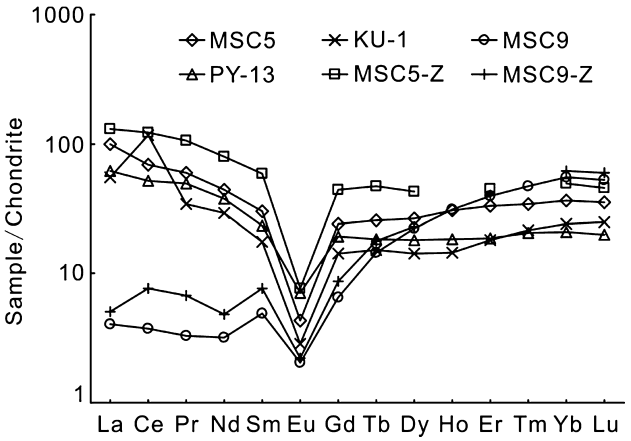

Fig. 5 Cl chondrite-normalized REE patterns of this study and the data cited for comparison (normalization values after McDonough and Sun 1995). KU-1 was after Pašava et al. (2010); PY-13 was after Zhou et al. (2014); MSC5-Z and MSC9-Z represent averages of K-bentonite samples from Bed 5 (K25, K27, K31) and K-bentonite samples from the bottom of Bed 9 (K108, K843), respectively, in the Meishucun section (data from Zhang et al. 1997)

are difficult to purify and result in contamination by clay crucible materials in fusion (Qi and Huang 2013). In addition, interference from high Cu and Ni concentrations produced in the fire-assay fusion method will occur in the analysis of low-Ru, -Rh, and -Pd concentration samples; these uncertainties make the method unsuitable for analysis of samples with low PGE concentrations (Qi and Huang 2013). In this study, the improved digestion method for PGE analysis (Qi et al. 2011) is preferred based on its low blank, good agreement between sample analysis and recommended value, and suitability in low PGE concentration determination. To further ensure the reliability of data, the fire-assay fusion method was employed for comparison.

The total procedural reagent blanks of PGE analysis by the improved digestion method range from 0.008×10^{-9} g (Ru) to 0.033×10^{-9} g (Pd). Determined values of reference materials UMT-1 and WGB-1 agree well with the certified values. Besides slightly high Rh, the determined values of reference material TDB-1 also agree with the certified values (Table 3). These results ensure the quality of the data. Being ground again and mixed thoroughly, MSC5-M avoids the possible nugget effect of low sampling volume. Furthermore, the low standard deviations of multiple parallel and duplicate analyses (0.003–0.05, Table 3) ensure the duplication and stability of the PGE determination procedure, and provide reliable constraints for PGE concentrations of all single Bed 5 samples. Compared to the single sample of Bed 5, Pt concentrations of MSC5-M are evidently higher, probably owing to contamination from the stainless steel grinding pod in secondary grinding. Ru concentrations are higher than most single samples but are in agreement with MSC-3 and MSC-9; and Ir, Rh, and Pd concentrations match well with that of the single Bed 5 sample. Although Pt concentrations are slightly contaminated, total PGE of MSC5-M is still not more than 1.50×10^{-9}, approximately 1.8–2.8 times that of the single Bed 5 sample. In Table 4, a concordant result with the fire-assay fusion method is obtained by the method applied in this study, $\sum(\mathrm{Pt} + \mathrm{Pd}) < 0.90 \times 10^{-9}$. Results of multiple parallel and duplicated MSC5-M samples by the two methods agree well, albeit with differences in individual elements and individual samples, and both have low PGE concentrations ($\sum\mathrm{PGEs} < 1.50 \times 10^{-9}$). Therefore, results

Table 3 Blank level ($\times 10^{-9}$ g), detection limits (DL, $\times 10^{-9}$) and analytical results ($\times 10^{-9}$) of PGEs for reference materials and MSC5-M

Elements	Blank	DL (3σ)	UMT-1 Ultramafic ore tailings	Certified[a]	WGB-1 Gabbro	Certified[a]	TDB-1 Diabase	Certified[a]	MSC5-M (Mean ± S[b]) $N = 6$
Ir	0.009	0.004	8.21	8.8	0.16	0.3	0.11	0.15	0.012 ± 0.003
Ru	0.008	0.008	9.82	10.9	0.12	0.3	0.6	0.3	0.017 ± 0.004
Rh	0.009	0.006	9.54	9.5	0.22	0.32	0.51	0.7	0.015 ± 0.004
Pt	0.021	0.014	120	128	5.39	6.1	4.90	5.8 ± 1.1	0.95 ± 0.05
Pd	0.033	0.012	113	106	13.8	13.9	22.6	22.4 ± 1.4	0.39 ± 0.05

The detection limit ($\times 10^{-9}$) is calculated as three times the standard deviation of five individual procedural reagent blanks ($\times 10^{-9}$ g), divided by the sample mass

[a] Certified values followed Govindaraju (1994)

[b] S = Standard deviation

of low PGE concentrations in all K-bentonites in this study are deemed reliable.

4.2.2 Characters of PGE concentrations

As shown in Table 4, $\sum$PGE concentrations of single K-bentonite samples of Bed 5 vary in narrow ranges and are all less than 0.90×10^{-9}, with an average of 0.67×10^{-9} and mean $\sum$(Pt + Pd) concentrations about 0.60×10^{-9}, with concentrations of Pt and Pd 0.04–0.21 $\times 10^{-9}$ and 0.37–0.65 $\times 10^{-9}$, respectively. $\sum$PGE concentrations of K-bentonite of Bed 9 bottom are 0.35×10^{-9}, with $\sum$(Pt + Pd) concentrations about 0.33×10^{-9}, lower than that of Bed 5 samples. Results using the fire-assay fusion method reveal that $\sum$(Pt + Pd) concentrations of Bed 5 samples in the Meishucun section are not more than 0.7×10^{-9}, with Pt concentrations 0.1–0.2 $\times 10^{-9}$ and Pd concentrations lower than 0.5×10^{-9}. Results are consistent across these two methods.

5 Discussion

5.1 Source rocks and alterations

Bed 5 K-bentonite of the Meishucun section mainly consists of claystones of illite and mixed-layered illite–smectite, with crystal fragments of quartz and biotite, and occasional zircon. SiO_2 contents of this layer are in the range of medium-acid magma. Meanwhile, samples generally have high K_2O (all >3.5 %) contents, high concentrations of lithophile elements (Hf, Ta, Th, Y, and U), and the volcanic activity marker element As, with characteristic TiO_2/Al_2O_3, Zr/Hf, Ti/Th ratios and similar granitic REE distribution patterns. Based on these characteristics, Bed 5 K-bentonites are suggested to have formed when primary acid volcanic ash deposited in the ocean underwent hydrolysis, alteration, and diagenesis. Bed 9 bottom K-bentonite has similar petrological and geochemical characteristics to Bed 5, but with apparent weathering. Occurring on the large open pit of the Kunyang Phosphorite Mine, phosphate laminae at Bed 9 bottom are characterized by hardground structure, representing transient uplift and an exposed event. Yellowish Bed 9 K-bentonite uniformly overlying the hardground-phosphorite was possibly subjected to contemporary groundwater leaching and weathering. Geochemically, yellowish Bed 9 K-bentonite has low Sr concentrations, a high Rb/Sr ratio, and a REE distribution pattern of depleted LREE and enriched HREE, sometimes with a positive Ce anomaly (Zhang et al. 1997).

Previous C and O isotope research do not support the existence of late hydrothermal activity in Bed 5 of the Meishucun section; if such hydrothermal activity occurred, it was likely limited to early diagenesis (Pašava et al. 2010). Field observations associated with characteristics of petrography, mineralogy, and geochemistry also do not support late hydrothermal activity. Based on petrographic observation, Pašava et al. (2010) suggest Bed 5 (sample KU-1) contains dolomite-hosted carbonate veins. Furthermore, a few dolomite lenses and laminae were found in field work. An individual sample (MSC-4) in this study is characterized by barite mineralization. Therefore, we suggest that in diagenesis Bed 5 of the Meishucun section encountered inhomogeneous weak dolomite and barite mineralization, but was not subjected to other alterations. K-bentonite of Bed 9 bottom has undergone weathering, with petrological and geochemical characteristics distinct from Bed 5 samples.

Due to their immobility in supergene and altered environments, Zr, Ti, Nb, and Y can be used to probe magmatic affinity. In K-bentonite–relevant researches, Nb/Y vs. Zr/TiO_2 diagrams established by Winchester and Floyd (1977) have been extensively employed to preliminarily discern the magmatic affinity of K-bentonite (Huff et al. 1992, 1998; Wan et al. 2013; Zhou et al. 2011, 2014). On a Nb/Y

Table 4 Analytical results of PGEs for samples from the K-bentonite layer (Bed 5) in the Meishucun section at the Kunyang Phosphorite Mine in Yunnan Province ($\times 10^{-9}$)

Sample	Ir	Ru	Rh	Pt	Pd	∑PGE	∑(Pt + Pb)	Pt/Pd	Pd/Ir
The improved digestion technique following Qi et al. (2011)									
MSC-1	0.015	0.075	0.011	0.07	0.37	0.54	0.44	0.19	24.89
MSC-2	0.016	0.075	0.010	0.08	0.46	0.64	0.54	0.19	28.82
MSC-3	0.007	0.016	0.009	0.21	0.61	0.85	0.82	0.34	85.61
MSC-4	0.011	0.078	0.014	0.16	0.42	0.68	0.58	0.39	36.46
MSC-5	0.016	0.036	0.012	0.04	0.43	0.53	0.46	0.08	26.78
MSC-6	0.013	0.027	0.018	0.10	0.47	0.63	0.57	0.22	34.71
MSC-7	0.014	0.070	0.011	0.07	0.56	0.73	0.63	0.13	40.62
MSC-8	0.014	0.030	0.011	0.07	0.63	0.76	0.71	0.12	45.60
MSC-9	0.009	0.023	0.016	0.07	0.47	0.59	0.54	0.15	55.36
MSC-10	0.015	0.033	0.010	0.06	0.58	0.69	0.63	0.10	38.92
MSC-11	0.013	0.055	0.010	0.09	0.48	0.65	0.57	0.19	35.42
MSC-12	0.016	0.030	0.013	0.09	0.65	0.81	0.75	0.14	40.10
MSC5	0.013	0.046	0.012	0.09	0.51	0.67	0.60	0.18	38.39
MSC9	0.002	0.015	0.005	0.06	0.26	0.35	0.33	0.24	107.36
PY-13	0.093	0.126	0.045	0.76	1.92	2.94	2.68	0.39	20.62
Fire assay preconcentration									
MSC-1			<2	0.1	<0.5		<0.6		
MSC-2			<2	0.1	<0.5		<0.6		
MSC-3			<2	0.1	<0.5		<0.6		
MSC-4			<2	0.1	<0.5		<0.6		
MSC-5			<2	0.1	<0.5		<0.6		
MSC-6			<2	0.1	<0.5		<0.6		
MSC-7			<2	0.2	0.5		0.7	0.4	
MSC-8			<2	0.2	<0.5		<0.7		
MSC-9			<2	0.1	<0.5		<0.6		
MSC-10			<2	0.1	0.5		0.6	0.2	
MSC-11			<2	0.2	<0.5		<0.7		
MSC-12			<2	0.1	<0.5		<0.6		
PGE data from references for comparison									
KU-1	0.14	0.9	57.97	434.1	142	635.11	576.1	3.06	1014.29
B1	0.1	1	0.19	4.3	4.7	10.29	9	0.91	47
B2	0.33	1.6	0.5	11.2	10	23.63	21.2	1.12	30.30
CA	0.003	0.007	0.004	0.06	0.08	0.154	0.14	0.75	26.67
CFV				0.22	0.23	0.45	0.45	0.96	
NAV	1.119	6.714		26.071	23.5	57.404	49.571	1.11	21.01
ZY	0.6	1.9	0.3	18	20	40.8	38	0.9	33.33
HJW-1	1.7	23	25	295	300	644.7	595	0.98	176.47
HJW-2	3	5	20	405	380	813	785	1.07	126.67

Some PGE data cited from references are listed in the table for comparison: KU-1 was after Pašava et al. (2010); B1 and B2 represent continental tholeiites and alkali basalts respectively (Barnes and Maier 1999); CA represents acid rocks in East China (Chi and Yan 2006); CFV represents felsic volcanics in central East China (Gao et al. 1998); NAV represents the average of 14 acid volcanics in Namibia (Borg et al. 1988); ZY represents a black shale bearing polymetallic Ni-Mo-PGE in Zunyi, Guizhou (Luo et al. 2003); HJW-1 and HJW-2 represent polymetallic Ni-Mo-PGE layer and Ni-Mo ore, respectively, of the Wangjiawan mine in Zunyi, Guizhou (Mao et al. 2002)

versus Zr/TiO_2 diagram, Bed 5 samples of the Meishucun section in the Kunyang Phosphorite Mine all plot in the fields of rhyolite and rhyodacite (dacite) (Fig. 6), indicating that the K-bentonites of the study area are most likely derived from acid magma. This is in good agreement with previous K-bentonites analyzed from the same layer

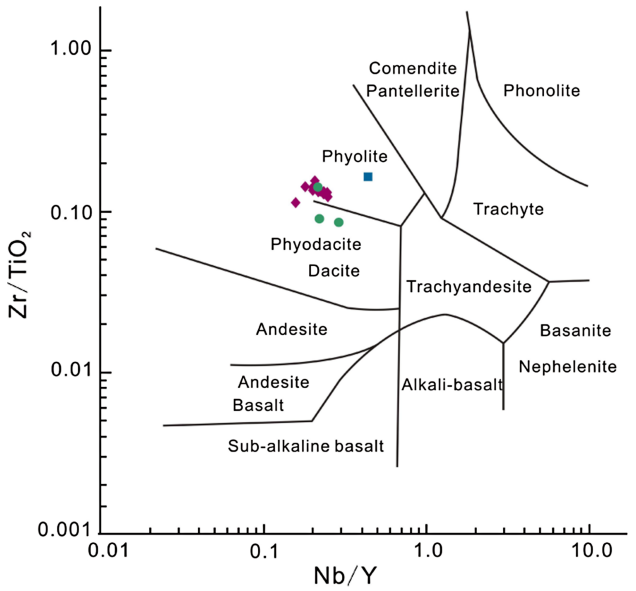

Fig. 6 Nb/Y versus Zr/TiO_2 diagram of this study and the data cited for comparison (after Winchester and Floyd 1977; Zhou et al. 2011). *Red diamonds* represent samples from Bed 5 of the Meishucun section; *green circles* represent samples from Bed 5 of the Meishucun section reported by Zhang et al. (1997); the *blue square* represents a sample from the deeper water facies of the Pingyin section in Jiangkou County, Guizhou Province, equivalent to Bed 5 of the Meishucun section (Zhou et al. 2013)

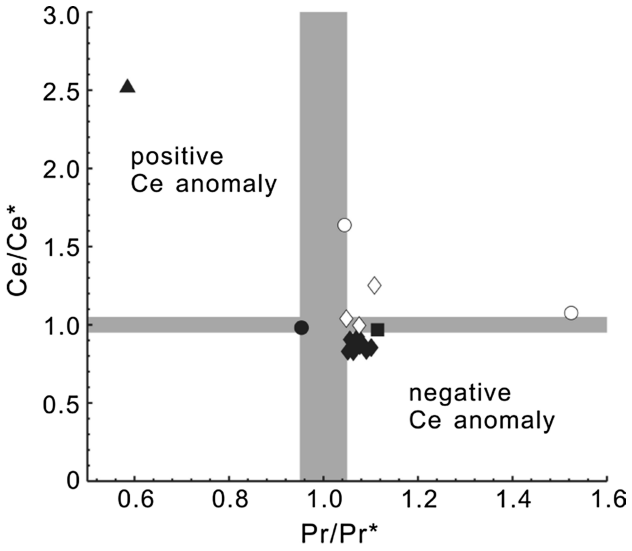

Fig. 7 Ce/Ce* versus Pr/Pr* diagram for this study and the data cited for comparison (modified after Bau and Dulski 1996). *Filled diamond* represent samples from the K-bentonite layer (Bed 5) in the Meishucun section for this study; *filled circle* represents sample MSC9; *filled triangle* represents a sample from the K-bentonite layer (Bed 5) in the Meishucun section reported by Pašava et al. (2010); *filled square* represents a sample from the deeper water facies of the Pingyin sectionin Jiangkou County, Guizhou Province, equivalent to Bed 5 of the Meishucun section (Zhou et al. 2013); symbols *open diamond* and *open circle* represent samples from the K-bentonite layer (Bed 5 and the *bottom* of Bed 9, respectively) in the Meishucun section reported by Zhang et al. (1997)

of the same section (Zhang et al. 1997) and the same layer of a different section (Zhou et al. 2013).

A La anomaly can interfere with the correct identification of a Ce anomaly (Bau and Dulski 1996); thus, a Ce/Ce* versus Pr/Pr* diagram is used to check the Ce anomaly in most of the relevant works. Ce anomaly is usually ascribed to redox conditions of deposition environments. As shown in Fig. 7, the slight negative Ce anomaly of Bed 5 samples of the Meishucun section of this study and previous work is consistent with the oxic condition of the shallow marine environment during phosphate deposition (Zeng and Yang 1987; Zeng et al. 1989; Yang et al. 1995), while Pašava et al. (2010) reported a considerable positive Ce anomaly for Bed 5 bottom K-bentonite (KU-1) of the same section. Pašava et al. (2010) attributed the Ce anomaly of KU-1 to the Ce-enriched minerals (most likely the phosphate grains and nodules) remaining when REEs associated with acid volcanic ash were leached in water–rock reactions after deposition. However, this perspective warrants debate, since (1) although phosphate grains and nodules precipitating Fe and Mn are likely to produce a positive Ce anomaly (Shields and Stille 2001), Fe and Mn contents of KU-1 are not high; the Fe content of KU-1 is lower than Bed 5 samples of this study; (2) a slight negative Ce anomaly is shown in this study, albeit in phosphorus matter (phosphate grains, Fig. 3), also exists in Bed 5 samples; and (3) negative– not positive–Ce anomalies are usually found in the Upper and Lower phosphorite and are mainly considered to be induced by variations in the local conditions of diagenesis (Shields and Stille 2001). It is inferred that the phosphorus matter possibly results in Ce depletion in water–rock reactions at some time after deposition. Field observations suggest Bed 5 bottom was locally oxidized and leached by groundwater, with grey-white K-bentonite converting to grey-yellow. KU-1 might represent the front of groundwater oxidizing and leaching, so it has a considerable positive Ce anomaly.

5.2 Discussion about PGE anomalies

KU-1 has anomalously high Pt and Pd concentrations (Pašava et al. 2010): 1973 and 617 times, respectively, those of felsic volcanic rocks (0.22×10^{-9} Pt, 0.23×10^{-9} Pd; Gao et al. 1998), reaching the level of PGE mineralization. In this study, total PGE concentrations of Bed 5 samples in the Meishucun section are all lower ($<0.90 \times 10^{-9}$), with the maximum Pt concentration (0.21×10^{-9}) comparable to felsic volcanic rock and Pd concentrations about 1.5–3 times those of felsic volcanic rocks (Gao et al. 1998), showing no anomaly. In deeper

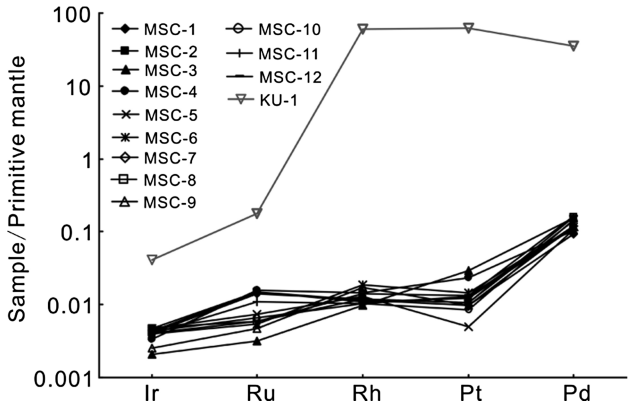

Fig. 8 Primitive mantle-normalized PGE patterns of samples of the K-bentonite layer (Bed 5) in the Meishucun section in the Kunyang Phosphorite Mine. KU-1 was after Pašava et al. (2010)

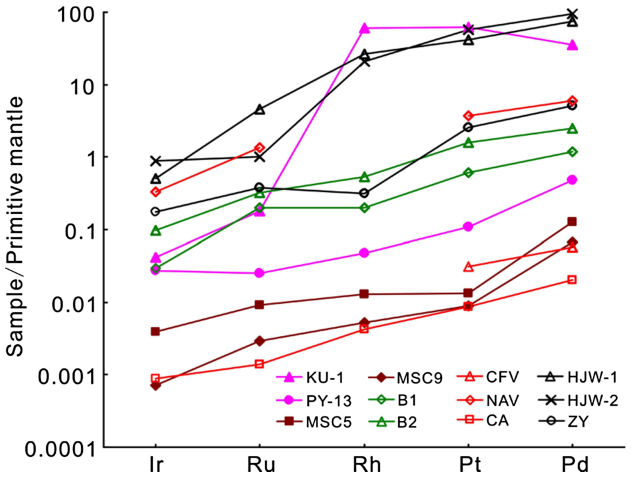

Fig. 9 Primitive mantle-normalized PGE patterns of this study and the data cited for comparison, including average K-bentonites from Bed 5 in the Meishucun section. KU-1 was after Pašava et al. (2010); B1 and B2 represent continental tholeiites and alkali basalts respectively (Barnes and Maier 1999); CA represents acid rocks in East China (Chi and Yan 2006); CFV represents felsic volcanics in central East China (Gao et al. 1998); NAV represents the average of 14 acid volcanics in Namibia (Borg et al. 1988); ZY represents a black shale bearing polymetallic Ni-Mo-PGE in Zunyi, Guizhou (Luo et al. 2003); HJW-1 and HJW-2 represent polymetallic Ni-Mo-PGE layer and Ni-Mo ore respectively of Wangjiawan mine in Zunyi, Guizhou (Mao et al. 2002)

water facies in Guizhou, the equivalent K-bentonite layer of Bed 5 of the Meishucun section has total PGE concentrations of 2.95×10^{-9}, Pt concentrations of 0.76×10^{-9}, and Pd concentrations of 1.92×10^{-9} (PY-13, Zhou et al. 2013, 2014). These are slightly higher than Bed 5 samples of this study, but well lower than Pašava et al. (2010), showing obvious PGE enrichment. The apparently weathered K-bentonite of Bed 9 bottom has total PGE concentrations of 0.35×10^{-9} and Pt and Pb concentrations of 0.06×10^{-9} and 0.26×10^{-9}, respectively. These values are lower than Bed 5 samples, and indicate no PGE anomaly.

Primitive-mantle-normalized PGE patterns of Bed 5 samples of the Meishucun section and relevant samples are generally consistent, with a left-tilt pattern (Figs. 8, 9) that IPGE are relatively depleted while PPGE are relatively enriched, and the only distinction is the extent of depletion or enrichment relative to primitive-mantle. However, the high enrichment of PPGE in KU-1 is outstanding. Comparing among the same layer samples (Bed 5 of the Meishucun section and its equivalent layers), PGE concentrations of Bed 5 K-bentonites are depleted relative to primitive mantle, with Pd/Ir of 24.89–85.61 averaging 38.39; relative to primitive mantle, KU-1 is depleted in Ir and Ru, but highly enriched in Rh and Pt, with a Pd/Ir ratio up to 1014.29. In deeper water facies, PGE concentrations of the equivalent layer (PY-13) of Bed 5 K-bentonite of the Meishucun section are wholly depleted relative to primitive mantle, but are slightly enriched relative to this study, with Pd/Ir of 20.62 similar to this study. Comparing the identical lithology of different layers as well as acid and basic rocks, it will find primitive-mantle-normalized PGE patterns of K-bentonites from Bed 5 and the bottom of Bed 9 in the Meishucun section approximately parallel to those of acid and basic rocks, but with different extents of depletion relative to primitive mantle (Namibia acid volcanic rocks are slightly enriched in Ru, Pt, and Pd; Borg et al. 1988). Compared to acid and basic rocks, most of the Pd/Ir ratios of Bed 5 are equal or slightly higher while Pt/Pd ratios are lower; the Pd/Ir ratio of weathered K-bentonite of Bed 9 bottom is several times higher, while the Pt/Pd ratio is comparable to Bed 5. In summary, K-bentonites from Bed 5 and the bottom of Bed 9 in the Meishucun section all have similar PGE characters; the main source of PGEs is original acid volcanic ash which is in agreement with previous work (Zhou et al. 2014), and weathering does not exert considerable influence on PGE concentration and differentiation.

The report of Pašava et al. (2010) shows that Bed 5 bottom sample (KU-1) is extremely enriched in PGEs. The concentrations of Rh, Pt, and Pd have reached the level of mineralization and the Pd/Ir and Pt/Pd ratios are both high (Pd/Ir is up to several tens of times higher), relative to normal acid rocks and slightly PGE-enriched acid rocks in Namibia. The special polymetallic Ni-Mo-PGE layer, hosted in black shale in the Zunyi district, generally equivalent to the middle of Bed 13 of the Meishucun section, has discontinuous lenticular and cystic sulfide ores containing Ni + Mo contents of up to 8 % and having apparent PGE mineralization. KU-1 is roughly equal to the Zhunyi Ni-Mo mine in terms of Pt and Pd content, but has a primitive-mantle-normalized PGE pattern different from that of the Zhunyi Ni-Mo mine. The anomalous Pt and Pd

contents of the Zunyi Ni-Mo mine are consistent with the existence of large quantities of sulfides; however, so far no obvious sulfide enrichment is found in Bed 5.

Volcanic ash precipitating from the atmosphere scatters extensively and has stable layers (Zhang et al. 1997). The thickness of volcanic ash precipitated during the same period does not generally differ much amongst locations in close proximity to one another. The typical thickness of volcanic ash preserved as K-bentonite in strata is about 10 cm. For example, the thickness of K-bentonite (Bed 5) of the Wangjiawan section, 23 km southeast of the Meishucun section, is about 10 cm (Zhou et al. 2014). However, although the Meishucun section is located not far away from the Wangjiawan section, its Bed 5 K-bentonite not only has a large average thickness (1.6 m), but also has highly variable thickness across the Kunyang Phosphorite Mine: the largest thickness we found is up to 4.5 m and the thickness of the sampling profile is about 3.5 m. Previous research suggests that the East Yunnan district was located in bay and lagoon environments between the central Yunnan Oldland and Niushoushan Palaeo-island (Oldland) during the Zhongyicun phosphorite depositon (Zeng and Yang 1987; Zeng et al. 1989; Zhang et al. 1997). Besides nutrient-rich seawater upwelling induced by tectonics (Shen et al. 2000), surface runoff from both the oldlands with high phosphorus background values also partially serves as a source for phosphorus matter in the Meishucun section (Zeng and Yang 1987). It can be deduced that the volcanic ash preserved in the Meishucun section, in addition to in situ precipitation, emanated in large proportion from the volcanic ash precipitating on nearby oldlands carried by surface runoff, was rapidly deposited in the Kunyang phosphorite district and rearranged by littoral currents, and finally developed into a layer much thicker than that of the nearby Wangjiawan section. During the hydrodynamic processes, the original volcanic ash likely developed local PGE-bearing mineral enrichment resulting in an extremely inhomogeneous distribution of PGEs. KU-1 was sampled from the bottom of this layer, and possibly was located exactly at the point of greatest PGE enrichment. Therefore, the anomalous PGE enrichment in KU-1 analyzed by Pašava et al. (2010) is most likely a nugget effect resulting from the transport of original volcanic ash, which does not indicate a generality in K-bentonite in the Meishucun section and its equivalent layers across South China.

6 Conclusions

Based on detailed field work and microscopic observations as well as systematic geochemical analysis of multiple samples—especially precise PGE determination—it can be concluded that:

(1) According to the petrology and mineralogy, as well as the major and trace element compositions, the original rock type of Bed 5 K-bentonite of the Meishucun section in the Kunyang Phosphorite Mine, Yunnan, is acid volcanic ash, including in situ volcanic ash and that carried by surface runoff. Under the rearrangement of littoral currents, anomalously thick K-bentonite developed in the Meishucun Sect.

(2) Quality of PGE analysis data were ensured by comparing results using two analysis methods, comparing results with reference materials, and running duplicate and parallel samples. The result of Bed 5 K-bentonite analysis is: PGE concentrations of all samples are lower than 0.90×10^{-9}, with an average of 0.67×10^{-9}; Pt + Pd concentration is not higher than 0.70×10^{-9}, with an average of 0.60×10^{-9}.

(3) The anomalous PGE enrichment of Bed 5 K-bentonite in the Meishucun section in the report of Pašava et al. (2010) differs significantly from the result of the same period deeper water facies K-bentonite, and also disagrees with the PGE evolution rule of acid magma. It is most likely that the nugget effect produced these results, and that no generality of PGE enrichment exists.

Acknowledgments Thanks are given for the help of Assist Prof. Huang Xiaowen and Assist Engineer Yin Yifan in PGE determination and the constructive advice offered by Prof. LuoTaiyi. We are grateful to the valuable suggestions and comments given by the anonymous reviewer. Thanks go to Dr. He Hongtao for the language polishing. This research is financially supported by National Science Foundation of China (Nos. 41072054, 40963002).

References

Barnes SJ, Maier WD (1999) The fractionation of Ni, Cu and the noble metals in silicate and sulfide liquids. In: Keays RR,Lesher CM, Lightfoot PC, Farrow CEG (eds) Dynamic processes in magmatic ore deposits and their application to mineral exploration, short course notes, vol 13. Geological Association of Canada, pp 69–106

Bau M, Dulski P (1996) Distribution of yttrium and rare-earth elements in the Penge and Kuruman iron-formations, Transvaal Supergroup, South Africa. Precambr Res 79(1–2):37–55

Borg G, Tredoux M, Maiden KJ, Sellschop JPF, Wayward OFD (1988) PGE- and Au-distribution in rift-related volcanics, sediments and stratabound Cu/Ag ores of middle Proterozoic age in central SWA/Namibia. In: Prichard HM, Potts PJ, Bowles JFW, Cribb SJ (eds) Geo-platinum 87. Springer Netherlands, pp 303–317

Brasier MD, Magaritz M, Corfield R, Luo H, Wu X, Ouyang L, Jiang Z, Hamdi B, He T, Fraser AG (1990) The carbon- and oxygen-isotope record of the Precambrian-Cambrian boundary interval in China and Iran and their correlation. Geol Mag 127(04):319–332

Chen D, Wang J, Qing H, Yan D, Li R (2009) Hydrothermal venting activities in the Early Cambrian, South China: petrological, geochronological and stable isotopic constraints. Chem Geol 258(3):168–181

Chi Q, Yan M (2006) Platinum-group element abundances in crust, rocks and sediments. Geochimica 35(5):461–471 **(in Chinese with English abstract)**

Compston W, Williams IS, Kirschvink JL, Zhang Z, Ma G (1992) Zircon U-Pb ages for the Early Cambrian time-scale. J Geol Soc 149(2):171–184

Compston W, Zhang Z, Cooper JA, Ma G, Jenkins RJF (2008) Further SHRIMP geochronology on the early Cambrian of South China. Am J Sci 308(4):399–420

Cook PJ, Shergold JH (1984) Phosphorus, phosphorites and skeletal evolution at the Precambrian–Cambrian boundary. Nature 308: 231–236

Cowie JW (1985) Continuing work on the Precambrian–Cambrian boundary. Episodes 8(2):93–97

Crimes TP, Jiang Z (1986) Trace fossils from the Precambrian–Cambrian boundary candidate at Meishucun, Jinning, Yunnan, China. Geol Mag 123(06):641–649

Feng B (1989) Carboniferous-Permian tonsteins formed by hydrolytic reformation of volcanic ash sediments in northern China. Acta Sedimentol Sin 7(1):101–108 **(in Chinese with English abstract)**

Feng B, Dong R (1993) Trace element Geochemistry of volcanic-sedimentary claystone and its source magma type and chemical differentiation mechanism. Reg Geol China 4:348–355 **(in Chinese with English abstract)**

Gao S, Luo T, Zhang B, Zhang H, Han Y, Zhao Z, Hu Y (1998) Chemical composition of the continental crust as revealed by studies in East China. Geochim Cosmochim Acta 62(11):1959–1975

Govindaraju K (1994) Compilation of working values and sample description for 383 geostandards. Geostand Newsl 18(S1):1–158

Huff WD, Bergström SM, Kolata DR (1992) Gigantic Ordovician volcanic ash fall in North America and Europe: biological, tectonomagmatic, and event-stratigraphic significance. Geology 20(10):875–878

Huff WD, Bergström SM, Kolata DR, Sun H (1998) The Lower Silurian Osmundsberg K-bentonite. Part II: mineralogy, geochemistry, chemostratigraphy and tectonomagmatic significance. Geol Mag 135(01):15–26

Jenkins RJF, Cooper JA, Compston W (2002) Age and biostratigraphy of Early Cambrian tuffs from SE Australia and southern China. J Geol Soc 159:645–658

Jiang S, Yang J, Ling H, Chen Y, Feng H, Zhao K, Ni P (2007) Extreme enrichment of polymetallic Ni–Mo–PGE–Au in Lower Cambrian black shales of South China: an Os isotope and PGE geochemical investigation. Palaeogeogr Palaeoclimatol Palaeoecol 254(1–2):217–228

Luo H, Jiang Z, Wu X, Song X, Ouyang L, Xing Y, Liu G, Zhang S, Tao Y (1984) Sinian-Cambrian boundary stratotype section at Meishucun, Jinning, Yunnan, China. People's Publishing House, Kunming, pp 65–110

Luo H, Jiang Z, Wu X, Song X, Ouyang L, Xing Y, Liu G, Zhang S, Tao Y (1985) Precambrian-Cambrian boundary section at Meishucun, Yunnan, China. Chin Sci Bull 30(21):1650–1652 **(in Chinese)**

Luo H, Jiang Z, Wu X, Ouyang L, Song X, Xue X (1991) A further research on the Precambrian-Cambrian boundary at the Meishucun section of Jinning, Yunnan. Acta Geola Sinica. 65(4): 367–375 **(in Chinese with English abstract)**

Luo H, Jiang Z, Tang L (1994) Stratotype section for Lower Cambrian stages in China. Yunnan Science and Technology Press, Kunming, pp 1–183 **(in Chinese with English abstract)**

Luo T, Zhang H, Li X, Zhu D (2003) Mineralization characteristics of the multi-element-rich strata in the Niutitang Formation black shale series, Zunyi, Guizhou, China. Acta Mineralogica Sinica 23(4):296–302 **(in Chinese with English abstract)**

Luo T, Ning X, Luo Y, Li X, Ling R, Yao L (2005) Super-enrichment of Se in the bottom black shales Lower Cambrian at Zunyi, Guizhou Province, China. Acta Mineralogica Sinica 25(3):275–282 **(in Chinese with English abstract)**

Mao J, Lehmann B, Du A, Zhang G, Ma D, Wang Y, Zeng M, Kerrich R (2002) Re-Os dating of polymetallic Ni-Mo-PGE-Au mineralization in Lower Cambrian black shales of South China and its geologic significance. Econ Geol 97(5):1051–1061

McDonough WF, Sun SS (1995) The composition of the Earth. Chem Geol 120(3–4):223–253

Parkhaev PY, Demidenko YE (2010) Zooproblematica and mollusca from the Lower Cambrian Meishucun section (Yunnan, China) and taxonomy and systematics of the Cambrian small shelly fossils of China. Paleontol J 44(8):883–1161

Pašava J, Frimmel H, Luo T, Koubová M, Martínek K (2010) Extreme PGE concentrations in Lower Cambrian acid tuff layer from the Kunyang phosphate deposit, Yunnan Province, South China—possible PGE source for Lower Cambrian Mo-Ni-polyelement ore beds. Econ Geol 105(6):1047–1056

Qi L, Huang X (2013) A review on Platinum-group elements and Re-Os isotopic analyses of geological samples. Bull Mineral Petrol Geochem 32(2):171–189 **(in Chinese with English abstract)**

Qi L, Hu J, Gregoire DC (2000) Determination of trace elements in granites by inductively coupled plasma mass spectrometry. Talanta 51(3):507–513

Qi L, Zhou M, Wang CY (2004) Determination of low concentrations of platinum group elements in geological samples by ID-ICP-MS. J Anal At Spectrom 19(10):1335–1339

Qi L, Zhou M, Wang CY, Sun M (2007) Evaluation of a technique for determining Re and PGEs in geological samples by ICP-MS coupled with a modified Carius tube digestion. Geochem J 41(6):407–414

Qi L, Gao J, Huang X, Hu J, Zhou M, Zhong H (2011) An improved digestion technique for determination of platinum group elements in geological samples. J Anal At Spectrom 26(9): 1900–1904

Qian Y, Yu W, Liu D, Wang Z (1984) A further research on the Sinian-Cambrian boundary section at Meishucun, Jinning, Yunnan. Chin Sci Bull 29(15):928–931 **(in Chinese)**

Sawaki Y, Nishizawa M, Suo T, Komiya T, Hirata T, Takahata N, Sano Y, Han J, Kon Y, Maruyama S (2008) Internal structures and U-Pb ages of zircons from a tuff layer in the Meishucunian formation, Yunnan Province, South China. Gondwana Res 14(1):148–158

Shen Y, Schidlowski M, Chu X (2000) Biogeochemical approach to understanding phosphogenic events of the terminal Proterozoic to Cambrian. Palaeogeogr Palaeoclimatol Palaeoecol 158(1): 99–108

Shields G, Stille P (2001) Diagenetic constraints on the use of cerium anomalies as palaeoseawater redox proxies: an isotopic and REE study of Cambrian phosphorites. Chem Geol 175(1–2):29–48

Song X (1984) Obruchevella from the early Cambrian Meishucun Stage of the Meishucun section, Jinning, Yunnan, China. Geol Mag 121(03):179–183

Steiner M, Li G, Qian Y, Zhu M, Erdtmann BD (2007) Neoproterozoic to early Cambrian small shelly fossil assemblages and a revised biostratigraphic correlation of the Yangtze Platform (China). Palaeogeogr Palaeoclimatol Palaeoecol 254(1):67–99

Su W, He L, Wang Y, Gong S, Zhou H (2003) K-bentonite beds and high-resolution integrated stratigraphy of the uppermost Ordovician Wufeng and the lowest Silurian Longmaxi formations in South China. Sci China Ser D 46(11):1121–1133

Turekian KK, Wedepohl KH (1961) Distribution of the elements in some major units of the earth's crust. Geol Soc Am Bull 72(2):175–192

Wan B, Guan C, Zhou C, Meng F, Pang K, Tang Q, Rao X (2013) Petrologic and geochemical characteristics of K-bentonites from the basal Ediacaran in Yangtze Platform, South China and their geological significance. Acta Petrologica Sinica 29(12):4373–4386 **(in Chinese with English abstract)**

Winchester JA, Floyd PA (1977) Geochemical discrimination of different magma series and their differentiation products using immobile elements. Chem Geol 20:325–343

Xu L, Lehmann B, Zhang X, Zheng W, Meng Q (2014) Trace element distribution in black shales from Kunyang phosphorite deposit and its geological significances. Acta Petrologica Sinica 30(6):1817–1827 **(in Chinese with English abstract)**

Yang W, Qi L, Lu X (1995) Geochemical characteristics and origin of phosphoric sedimentary formation REE in Early Cambrian in the eastern Yunnan. Bull Mineral Petrol Geochem 12(4):224–227 **(in Chinese)**

Yang F, Xiao R, Xia X (2011) Sedimentary environment and geochemistry of the Kunyang phosphorite deposit in eastern Yunnan Province. Geol Explor 47(2):294–303 **(in Chinese with English abstract)**

Zeng Y, Yang W (1987) Meishucun of enrichment of Kunyang and Haikou phospharite deposits, Yunnan China. Acta Sedimentol Sin 5(3):19–28 **(in Chinese with English abstract)**

Zeng Y, Shen L, Ho T (1989) Sedimentary environment and minerogenentic mechanism of phosphorite ores in east Yunnan. Miner Rocks 9(2):45–59 **(in Chinese with English abstract)**

Zhang J, Li G, Zhou C (1997) Geochemistry of light colour clayrock layers from the Early Cambrian Meishucun stage in eastern Yunnan and their geological significance. Acta Petrologica Sinica 13(1):100–110 **(in Chinese with English abstract)**

Zhou M, Luo T, Huang Z, Long H, Yang Y (2007) Advances in research on K-bentonite. Acta Mineralogica Sinica 27(3/4):351–359 **(in Chinese with English abstract)**

Zhou M, Luo T, Li Z, Zhao H, Long H, Yang Y (2008) SHRIMP U-Pb zircon age of tuff at the bottom of the Lower Cambrian Niutitang Formation, Zunyi, South China. Chin Sci Bull 53(4):576–583

Zhou M, Luo T, Huang Z, Liu S (2011) Early Cambrian volcanic records in Guizhou Province, China and their geological significances. Acta Mineralogica Sinica 31(3):453–461 **(in Chinese with English abstract)**

Zhou M, Luo T, Liu S, Qian Z, Xing L (2013) SHRIMP zircon age for a K-bentonite in the top of the Laobao Formation at the Pingyin section, Guizhou, South China. Sci China Earth Sci 56(10):1677–1687

Zhou M, Luo T, Huff WD, Liu S (2014) Prominent Lower Cambrian K-bentonites in South China: distribution, mineralogy, and geochemistry. J Sediment Res 84(10):842–853

Zhu M, Zhang J, Steiner M, Yang A, Li G, Erdtmann BD (2003) Sinian-Cambrian stratigraphic framework for shallow- to deep-water environments of the Yangtze Platform: an integrated approach. Prog Nat Sci 13(12):951–960

Zhu R, Li X, Hou X, Pan Y, Wang F, Deng C, He H (2009) SIMS U-Pb zircon age of a tuff layer in the Meishucun section, Yunnan, southwest China: constraint on the age of the Precambrian–Cambrian boundary. Sci China Ser D 52(9):1385–1392